arXiv:1604.08906v1 [cond-mat.mes-hall] 29 Apr 2016

Controllable Goos-Hänchen Shift in Graphene Triangular Double Barrier

Miloud Mekkaoui[a], **Ahmed Jellal**[*a,b] and **Hocine Bahlouli**[b,c]

[a] *Theoretical Physics Group, Faculty of Sciences, Chouaïb Doukkali University, PO Box 20, 24000 El Jadida, Morocco*

[b] *Saudi Center for Theoretical Physics, Dhahran, Saudi Arabia*

[c] *Physics Department, King Fahd University of Petroleum & Minerals, Dhahran 31261, Saudi Arabia*

Abstract

We study the Goos-Hänchen shifts for Dirac fermions in graphene scattered by a triangular double barrier potential. The massless Dirac-like equation was used to describe the scattered fermions by such potential configuration. Our results show that the GHL shifts is affected by the geometrical structure of the double barrier. In particular the GHL shifts change sign at the transmission zero energies and exhibit enhanced peaks at each bound state associated with the double barrier when the incident angle is less than the critical angle associated with the total reflection.

PACS numbers: 72.80.Vp, 73.21.-b, 71.10.Pm, 03.65.Pm

Keywords: graphene, double barriers, scattering, Goos-Hänchen shifts.

[*] ajellal@ictp.it – a.jellal@ucd.ac.ma

1 Introduction

During the few past years there is a progress in studying electron transport properties in the graphene systems [1]. With this respect, we cite the quantum version of the Goos-Hänchen effect originating from the reflection of particles from interfaces. The Goos-Hänchen shift was discovered by Hermann Fritz Gustav Goos and Hilda Hänchen [2, 3] and theoretically explained by Artman [4] in the late of 1940s. Many works in various graphene-based nanostructures, including single [5], double barrier [6] and superlattices [7], showed that the Goos-Hänchen like (GHL) shifts can be enhanced by the transmission resonances and controlled by varying the electrostatic potential and induced gap [5]. Similar to those in semiconductors, the GHL shifts in graphene can also be modulated by the electric and magnetic barriers [8] as well as atomic optics [9]. It has been reported that the GHL shifts play an important role in the group velocity of quasiparticles along interfaces of graphene p-n junctions [10, 11].

Very recently, we have studied the Dirac fermions in graphene scattered by a triangular double barrier in terms of the transmission probability [12]. The system was made of two triangular potential barrier regions separated by a well region characterized by an energy gap G_p. Solving the Dirac-like equation and matching the solutions at the boundaries, the transmission and reflection coefficients were expressed in terms of transfer matrix. In particular, it is showed that the transmission exhibits oscillation resonances that are manifestation of the Klein tunneling effect.

Actually we are wondering to extend our work [12] to deal with other issues related to graphene systems. Indeed, we investigate the GHL shifts for a system made of graphene with gap an in presence of the triangular double barrier potential. By splitting our system into three regions, we determine the solutions of the energy spectrum in terms of different physical quantities. After matching the wave functions at both interfaces, we calculate the transmission coefficient as well as the GHL shifts. To give a better understanding of our results, we plot the GHL shifts versus various physical parameters characterizing our system.

The paper is organized as follows. In section 2, we formulate our model by setting the Hamiltonian system describing particles scattered by a triangular double barrier whose intermediate zone is subject to a mass term. In section 3, we obtain the spinor solution corresponding to each regions composing our system. We use the transfer matrix to describe the boundary conditions and split the energy regions into three domains in order to calculate the the phase shift and GHL shifts. In section 4, we numerically present our results for the GH shifts and the transmission probability of an electron beam transmitted through a graphene triangular double barrier. We then conclude our work in the final section.

2 System model

We consider a system of massless Dirac fermions through a strip of graphene with the Fermi energy E and the incidence angle ϕ_1 with respective to the incident x-direction of two-dimensional graphene sheet subject to a triangular double barrier potential. Specifically this system is a flat sheet of graphene subject to a square potential barrier along the x-direction while particles are free in the y-direction. For ease of mathematical formulation let us first describe the geometry of our system as being made of five regions denoted by $\mathrm{j} = 1, \cdots, 5$. Each region is characterized by its potential and interaction

with external sources. The barrier regions are formally described by a Dirac-like Hamiltonian

$$H = v_F \boldsymbol{\sigma} \cdot \mathbf{p} + V(x)\mathbb{I}_2 + \Delta\sigma_z \tag{1}$$

where $v_F \approx 10^6 m/s$ is the Fermi velocity, $\boldsymbol{\sigma} = (\sigma_x, \sigma_y)$ are the Pauli matrices, $\mathbf{p} = -i\hbar(\partial_x, \partial_y)$, $\mathbb{I}_2$ the 2×2 unit matrix, the electrostatic potential $V(x) = V_{\mathsf{j}}$ in each scattering region. The parameter $\Delta = mv_F^2$ is the energy gap originating either from sublattice symmetry breaking or from the spin-orbit interaction. It is defined by

$$\Delta = t'\Theta\left(d_1^2 - x^2\right) \tag{2}$$

where Θ is the Heaviside step function, d_1 and t' are positive numbers defining the width and strength of the energy gap region. In order to study the scattering of Dirac fermions in graphene by the above double barrier structure we first choose the following explicit potential configuration

$$V(x) = V_{\mathsf{j}} = \begin{cases} (\gamma x + d_2)F, & d_1 \le |x| \le d_2 \\ V_2, & |x| \le d_1 \\ 0, & \text{otherwise} \end{cases} \tag{3}$$

with d_1 is a positive number such that $d_2 - d_1$ represents the width of the triangular potential barrier region and $\gamma = \pm 1$, $\gamma = 1$ for $x \in [-d_2, -d_1]$, $\gamma = -1$ for $x \in [d_1, d_2]$ and $F = \frac{v_1}{d_2 - d_1}$.

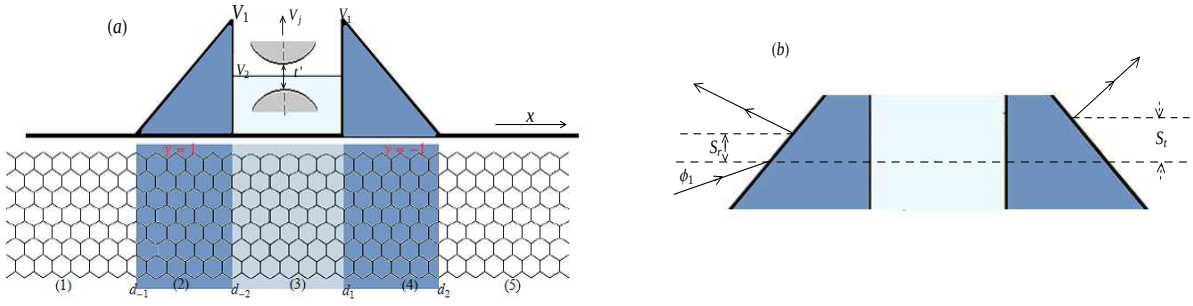

Figure 1: Schematic diagram for Dirac fermions in inhomogeneous magnetic field through a graphene double barrier, with the two barriers triangular of width $d_2 - d_1$ height V_1, and distance $2d_1$ height potential V_2 between them. (a): the dashed lines show smooth electric potentials with distributions of error functions. (b): describes the incident, reflected, and transmitted electron beams with a lateral shift S_r and S_t.

We define each potential region as follows: $\mathsf{j} = 1$ for $x \le -d_2$, $\mathsf{j} = 2$ for $-d_2 \le x \le -d_1$, $\mathsf{j} = 3$ for $-d_1 \le x \le d_1$, $\mathsf{j} = 4$ for $d_1 \le x \le d_2$ and $\mathsf{j} = 5$ for $x \ge d_2$. The corresponding constant potentials are given in (3) and are denoted by V_{j} in the j-th region, the five regions indicated schematically in Figure 1, which shows the space configuration of the potential profile. We therefore need to study just one $\mathbf{K}$ point. The time-independent Dirac equation for the spinor $\Phi(x, y) = (\varphi^+, \varphi^-)^T$, where T stands for the transpose and $E = v_F\epsilon$ is the energy of the system, which can be defined by

$$\left[\boldsymbol{\sigma} \cdot \mathbf{p} + v_{\mathsf{j}}\mathbb{I}_2 + \mu\Theta\left(d_1^2 - x^2\right)\sigma_z\right]\Phi(x, y) = \epsilon\Phi(x, y) \tag{4}$$

in the unit system $\hbar = 1$, with $V_{\mathsf{j}} = v_F v_{\mathsf{j}}$, $t' = v_F\mu$, $F = v_F\varrho$ and $V_1 = v_F v_1$. Our system is supposed to have finite width W with infinite mass boundary conditions on the wavefunction at the boundaries

$y = 0$ and $y = W$ along the y-direction [18, 25]. These boundary conditions result in a quantization of the transverse momentum along the y-direction

$$k_y = \frac{\pi}{W}\left(n + \frac{1}{2}\right), \qquad n = 0, 1, 2 \cdots . \tag{5}$$

One can therefore assume a spinor solution of the form $\Phi_{\mathsf{j}} = \left(\varphi_{\mathsf{j}}^{+}(x), \varphi_{\mathsf{j}}^{-}(x)\right)^{T} e^{ik_y y}$ and the subscripts $\mathsf{j} = 1, 2, 3, 4, 5$, indicates the space region while the superscripts indicate the two spinor components. Solving the eigenvalue equation to obtain the upper and lower components of the eignespinor in the incident and reflection region ($x < -d_2$)

$$\Phi_1 = \begin{pmatrix} 1 \\ z_1 \end{pmatrix} e^{i(k_1 x + k_y y)} + r_s \begin{pmatrix} 1 \\ -z_1^{-1} \end{pmatrix} e^{i(-k_1 x + k_y y)} \tag{6}$$

$$z_1 = s_1 \frac{k_1 + i k_y}{\sqrt{k_1^2 + k_y^2}} \tag{7}$$

where the sign function is defined by $s_{\mathsf{j}} = \mathrm{sign}(E)$. The corresponding dispersion relation is given by

$$\epsilon = s_1 \sqrt{k_1^2 + k_y^2}. \tag{8}$$

In region 2 and 4 ($d_1 < |x| < d_2$), the general solution can be expressed in terms of the parabolic cylinder function [19, 20, 24] as

$$\chi_\gamma^{+} = c_{n1} D_{\nu_n - 1}\left(Q_\gamma\right) + c_{n2} D_{-\nu_n}\left(-Q_\gamma^{*}\right) \tag{9}$$

where $\nu_n = \frac{i k_y^2}{2\varrho}$, $\epsilon_0 = \epsilon - v_1$, $Q_\gamma(x) = \sqrt{\frac{2}{\varrho}} e^{i\pi/4}\left(\gamma \varrho x + \epsilon_0\right)$, c_{n1} and c_{n2} are constants. The second component reads as

$$\chi_\gamma^{-} = -\frac{c_{n2}}{k_y}\left[2(\epsilon_0 + \gamma\varrho x) D_{-\nu_n}\left(-Q_\gamma^{*}\right) + \sqrt{2\varrho} e^{i\pi/4} D_{-\nu_n + 1}\left(-Q_\gamma^{*}\right)\right] - \frac{c_{n1}}{k_y}\sqrt{2\varrho} e^{-i\pi/4} D_{\nu_n - 1}\left(Q_\gamma\right) \tag{10}$$

The components of the spinor solution of the Dirac equation (4) in region 2 and 4 can be obtained from (9) and (10) with $\varphi_\gamma^{+}(x) = \chi_\gamma^{+} + i\chi_\gamma^{-}$ and $\varphi_\gamma^{-}(x) = \chi_\gamma^{+} - i\chi_\gamma^{-}$. In regions j=2,4 we have the eigenspinors

$$\Phi_{\mathsf{j}} = a_{\mathsf{j}-1} \begin{pmatrix} \eta_\gamma^{+}(x) \\ \eta_\gamma^{-}(x) \end{pmatrix} e^{ik_y y} + a_{\mathsf{j}} \begin{pmatrix} \xi_\gamma^{+}(x) \\ \xi_\gamma^{-}(x) \end{pmatrix} e^{ik_y y} \tag{11}$$

The function $\eta_\gamma^{\pm}(x)$ and $\xi_\gamma^{\pm}(x)$ are given by

$$\eta_\gamma^{\pm}(x) = D_{\nu_n - 1}\left(Q_\gamma\right) \mp \frac{1}{k_y}\sqrt{2\varrho} e^{i\pi/4} D_{\nu_n}\left(Q_\gamma\right) \tag{12}$$

$$\xi_\gamma^{\pm}(x) = \pm\frac{1}{k_y}\sqrt{2\varrho} e^{-i\pi/4} D_{-\nu_n + 1}\left(-Q_\gamma^{*}\right) \pm \frac{1}{k_y}\left(-2i\epsilon_0 \pm k_y - \gamma 2i\varrho x\right) D_{-\nu_n}\left(-Q_\gamma^{*}\right). \tag{13}$$

In region 2:

$$\Phi_2 = a_1 \begin{pmatrix} \eta_1^{+}(x) \\ \eta_1^{-}(x) \end{pmatrix} e^{ik_y y} + a_2 \begin{pmatrix} \xi_1^{+}(x) \\ \xi_1^{-}(x) \end{pmatrix} e^{ik_y y} \tag{14}$$

In region 4:

$$\Phi_4 \;=\; a_3 \begin{pmatrix} \eta^{+}_{-1}(x) \\ \eta^{-}_{-1}(x) \end{pmatrix} e^{ik_y y} + a_4 \begin{pmatrix} \xi^{+}_{-1}(x) \\ \xi^{-}_{-1}(x) \end{pmatrix} e^{ik_y y} \tag{15}$$

where $\gamma = \pm 1$. Solving the eigenvalue equation for the Hamiltonian (4) describing region 3, we find the following eigenspinor

$$\Phi_3 = b_1 \begin{pmatrix} \alpha \\ \beta z_3 \end{pmatrix} e^{i(k_3 x + k_y y)} + b_2 \begin{pmatrix} \alpha \\ -\beta z_3^{-1} \end{pmatrix} e^{i(-k_3 x + k_y y)} \tag{16}$$

with the parameters α and β are defined by

$$\alpha = \left(1 + \frac{\mu}{\epsilon - v_2}\right)^{1/2}, \qquad \beta = \left(1 - \frac{\mu}{\epsilon - v_2}\right)^{1/2} \tag{17}$$

and the complex number

$$z_3 = s_3 \frac{k_3 + i k_y}{\sqrt{k_3^2 + k_y^2}} \tag{18}$$

with the sign function $s_3 = \mathrm{sign}(\epsilon - v_2)$. The wave vector being

$$k_3 = \sqrt{(\epsilon - v_2)^2 - \mu^2 - {k_y}^2} \tag{19}$$

Finally the eigenspinor in region 5 ($x > d_2$) can be expressed as

$$\Phi_5 = t_s \begin{pmatrix} 1 \\ z_1 \end{pmatrix} e^{i(k_1 x + k_y y)}. \tag{20}$$

In the next, we will see how to use the above solutions in order to deal with different issues. These concern the transmission and reflection probabilities, which will allow us to determine the phase shift and therefore study the Goos-Hänchen like shifts.

3 Phase shift and GHL shifts

The transmission and reflection coefficients (r_s, t_s) can be determined using the boundary conditions and continuity of the eigenspinors at each interface. These will help to build a bridge between quantum optics and Dirac fermions in graphene through the GHL shifts. We prefer to express these relationships in terms of 2×2 transfer matrices between different regions $M_{j,j+1}$, such as

$$\begin{pmatrix} a_{\mathrm{j}} \\ b_{\mathrm{j}} \end{pmatrix} = M_{\mathrm{j,j+1}} \begin{pmatrix} a_{\mathrm{j+1}} \\ b_{\mathrm{j+1}} \end{pmatrix}. \tag{21}$$

From this, we finally end up with the full transfer matrix over the whole double barrier which can be written, in an obvious notation, as

$$\begin{pmatrix} 1 \\ r_s \end{pmatrix} = \prod_{\mathrm{j}=1}^{4} M_{\mathrm{jj+1}} \begin{pmatrix} t_s \\ 0 \end{pmatrix} = M \begin{pmatrix} t_s \\ 0 \end{pmatrix} \tag{22}$$

where the total transfer matrix $M = M_{12} \cdot M_{23} \cdot M_{34} \cdot M_{45}$ and $M_{\mathsf{jj+1}}$ are transfer matrices that couple the wave function in the j-th region to the wave function in the $(\mathsf{j}+1)$-th region. These are given explicitly by

$$M = \begin{pmatrix} m_{11} & m_{12} \\ m_{21} & m_{22} \end{pmatrix} \tag{23}$$

$$M_{12} = \begin{pmatrix} e^{-ik_1 d_2} & e^{ik_1 d_2} \\ z_1 e^{-ik_1 d_2} & -z_1^* e^{ik_1 d_2} \end{pmatrix}^{-1} \begin{pmatrix} \eta_1^+(-d_2) & \xi_1^+(-d_2) \\ \eta_1^-(-d_2) & \xi_1^-(-d_2) \end{pmatrix} \tag{24}$$

$$M_{23} = \begin{pmatrix} \eta_1^+(-d_1) & \xi_1^+(-d_1) \\ \eta_1^-(-d_1) & \xi_1^-(-d_1) \end{pmatrix}^{-1} \begin{pmatrix} \alpha e^{-ik_3 d_1} & \alpha e^{ik_3 d_1} \\ \beta z_3 e^{-ik_3 d_1} & -\beta z_3^* e^{ik_3 d_1} \end{pmatrix} \tag{25}$$

$$M_{34} = \begin{pmatrix} \alpha e^{ik_3 d_1} & \alpha e^{-ik_3 d_1} \\ \beta z_3 e^{ik_3 d_1} & -\beta z_3^* e^{-ik_3 d_1} \end{pmatrix}^{-1} \begin{pmatrix} \eta_{-1}^+(d_1) & \xi_{-1}^+(d_1) \\ \eta_{-1}^-(d_1) & \xi_{-1}^-(d_1) \end{pmatrix} \tag{26}$$

$$M_{45} = \begin{pmatrix} \eta_{-1}^+(d_2) & \xi_{-1}^+(d_2) \\ \eta_{-1}^-(d_2) & \xi_{-1}^-(d_2) \end{pmatrix}^{-1} \begin{pmatrix} e^{ik_1 d_2} & e^{-ik_1 d_2} \\ z_1 e^{ik_1 d_2} & -z_1^* e^{-ik_1 d_2} \end{pmatrix} \tag{27}$$

with the following relationships between the parabolic cylindrical functions

$$\eta_{-1}^{\pm}(d_1) = \eta_1^{\pm}(-d_1), \qquad \eta_{-1}^{\pm}(d_2) = \eta_1^{\pm}(-d_2) \tag{28}$$

$$\xi_{-1}^{\pm}(d_1) = \xi_1^{\pm}(-d_1), \qquad \xi_{-1}^{\pm}(d_2) = \xi_1^{\pm}(-d_2). \tag{29}$$

The above analysis allows to extract the transmission and reflection amplitudes as

$$t_s = \frac{1}{m_{11}}, \qquad r_s = \frac{m_{21}}{m_{11}}. \tag{30}$$

At this stage, we should point out that we were unfortunately forced to adopt a somehow cumbersome notation for our wavefunction parameters in different potential regions due to the relatively large number of necessary subscripts and superscripts. Before matching the eigenspinors at the boundaries, let us define the following shorthand notation

$$\eta_1^{\pm}(-d_1) = \eta_{11}^{\pm}, \qquad \eta_1^{\pm}(-d_2) = \eta_{12}^{\pm} \tag{31}$$

$$\xi_1^{\pm}(-d_1) = \xi_{11}^{\pm}, \qquad \xi_1^{\pm}(-d_2) = \xi_{12}^{\pm} \tag{32}$$

Now we are able to explicitly determine the transmission amplitude t_s. Indeed, after some lengthy algebra, one can solve the linear system given in (22) to obtain the transmission and reflection amplitudes in closed form. We obtain

$$t_s = \frac{\alpha\beta e^{2i(k_1 d_2 + k_3 d_1)} \left(1 + z_1^2\right)\left(1 + z_3^2\right)}{z_3 \left(e^{4ik_3 d_1} - 1\right)\left(\alpha^2 G_2 + \beta^2 G_1\right) + \alpha\beta G_3} \left(\xi_{11}^+ \eta_{11}^- - \xi_{11}^- \eta_{11}^+\right)\left(\xi_{12}^- \eta_{12}^+ - \xi_{12}^+ \eta_{12}^-\right) \tag{33}$$

where we have defined the following quantities

$$G_1 = \left(\xi_{12}^- \eta_{11}^+ - \xi_{11}^+ \eta_{12}^- - \xi_{12}^+ \eta_{11}^+ z_1 + \xi_{11}^+ \eta_{12}^+ z_1\right)\left(\xi_{11}^+ \eta_{12}^+ + \xi_{11}^+ \eta_{12}^- z_1 - \eta_{11}^+ (\xi_{12}^+ + \xi_{12}^- z_1)\right) \tag{34}$$

$$G_2 = \left(\xi_{11}^- \eta_{12}^+ - \xi_{11}^- \eta_{12}^- z_1 - \eta_{11}^- (\xi_{12}^+ + \xi_{12}^+ z_1)\right)\left(-\xi_{12}^- \eta_{11}^- + \xi_{12}^+ \eta_{11}^- z_1 - \xi_{11}^- (\eta_{12}^- + \eta_{12}^+ z_1)\right) \tag{35}$$

$$G_3 = \Gamma_0 \left(1 + z_1^2 z_3^2\right) + \Gamma_1 z_1 \left(1 - z_3\right) + \Gamma_2 \left(z_1^2 + z_3^2\right) + e^{4id_1 k_3} \left(\Gamma_3 + \Gamma_4\right) \tag{36}$$

as well as

$$\begin{aligned}
\Gamma_0 &= -\xi_{12}^{+}\xi_{12}^{-}\eta_{11}^{+}\eta_{11}^{-}+\xi_{11}^{+}\xi_{12}^{-}\eta_{11}^{-}\eta_{12}^{+}+\xi_{11}^{-}\xi_{12}^{+}\eta_{11}^{+}\eta_{12}^{-}-\xi_{11}^{+}\xi_{11}^{-}\eta_{12}^{+}\eta_{12}^{-} && (37)\\
\Gamma_1 &= \left(\xi_{12}^{+}\right)^2\eta_{11}^{+}\eta_{11}^{-}-\left(\xi_{12}^{-}\right)^2\eta_{11}^{+}\eta_{11}^{-}-\xi_{11}^{-}\xi_{12}^{+}\eta_{11}^{+}\eta_{12}^{+}-\xi_{11}^{+}\xi_{12}^{+}\eta_{11}^{-}\eta_{12}^{+} && (38)\\
&\quad +\xi_{11}^{+}\xi_{11}^{-}\left(\eta_{12}^{+}\right)^2-\xi_{11}^{+}\xi_{11}^{-}\left(\eta_{12}^{-}\right)^2+\xi_{11}^{-}\xi_{12}^{-}\eta_{11}^{+}\eta_{12}^{-}+\xi_{11}^{+}\xi_{12}^{-}\eta_{11}^{-}\eta_{12}^{-} &&\\
\Gamma_2 &= \xi_{12}^{+}\xi_{12}^{-}\eta_{11}^{+}\eta_{11}^{-}-\xi_{11}^{-}\xi_{12}^{-}\eta_{11}^{+}\eta_{12}^{+}-\xi_{11}^{+}\xi_{12}^{+}\eta_{11}^{-}\eta_{12}^{-}+\xi_{11}^{+}\xi_{11}^{-}\eta_{12}^{+}\eta_{12}^{-} && (39)\\
\Gamma_3 &= \left(\xi_{12}^{+}\right)^2\eta_{11}^{+}\eta_{11}^{-}\left(z_3^2-1\right)-\xi_{11}^{-}\xi_{12}^{-}\eta_{11}^{+}\left[\eta_{12}^{+}\left(1+z_1^2z_3^2\right)-\eta_{12}^{-}z_1\left(z_3^2-1\right)\right] && (40)\\
&\quad +\xi_{11}^{-}\xi_{11}^{+}\left[\left(\eta_{12}^{+}\right)^2z_1-\left(\eta_{12}^{-}\right)^2z_1+\eta_{12}^{+}\eta_{12}^{-}\left(z_1^2-1\right)\left(z_3^2-1\right)\right] &&\\
\Gamma_4 &= \xi_{12}^{-}\eta_{11}^{-}\left[-\xi_{12}^{-}\eta_{11}^{+}z_1\left(z_3^2-1\right)+\xi_{11}^{+}\left(\eta_{12}^{-}z_0\left(z_3^2-1\right)+\eta_{12}^{+}\left(z_1^2+z_3^2\right)\right)\right] && (41)\\
&\quad \xi_{12}^{+}\xi_{12}^{-}\eta_{11}^{+}\eta_{11}^{-}\left(z_1^2+1\right)\left(z_1^3-1\right)-\xi_{12}^{+}\xi_{11}^{+}\eta_{11}^{-}\left(\eta_{12}^{-}\left(1+z_1^2z_3^2\right)+\eta_{12}^{+}z_1\left(z_1^3-1\right)\right) &&\\
&\quad +\xi_{12}^{+}\xi_{11}^{-}\eta_{11}^{+}\left[\eta_{12}^{-}\left(z_1^2+z_3^2\right)+\eta_{12}^{+}z_1\left(1-z_3^2\right)\right] &&
\end{aligned}$$

The transmission and reflection amplitudes can be expressed as complex numbers

$$t_s = \rho_{t_s}e^{i\varphi_{t_s}} \tag{42}$$

$$r_s = \rho_{r_s}e^{i\varphi_{r_s}} \tag{43}$$

where we have defined the phase shift of the transmission and reflection amplitudes as being φ_t and φ_r, respectively

$$\varphi_{t_s} = \arctan\left(\frac{\Im[t_s]}{\Re[t_s]}\right), \qquad \varphi_{r_s} = \arctan\left(\frac{\Im[r_s]}{\Re[r_s]}\right) \tag{44}$$

as well as the amplitudes

$$\rho_{t_s} = \left(\Re[t_s]^2+\Im[t_s]^2\right)^{\frac{1}{2}}, \qquad \rho_{r_s} = \left(\Re[r_s]^2+\Im[r_s]^2\right)^{\frac{1}{2}} \tag{45}$$

with as usual the real and imaginary parts are given by

$$\Re[t_s] = \frac{t_s+t_s^*}{2}, \qquad \Im[t_s] = \frac{t_s-t_s^*}{2i} \tag{46}$$

$$\Re[r_s] = \frac{r_s+r_s^*}{2}, \qquad \Im[r_s] = \frac{r_s-r_s^*}{2i}. \tag{47}$$

These allow us to express the phase shift as

$$\varphi_{t_s} = \arctan\left(i\frac{t_s^*-t_s}{t_s+t_s^*}\right), \qquad \varphi_{r_s} = \arctan\left(i\frac{r_s^*-r_s}{r_s+r_s^*}\right). \tag{48}$$

We study GHL shifts in graphene by considering an incident, reflected and transmitted beams with some transverse wave vector $k_y = k_{y_0}$ and angle of incidence $\phi_1(k_{y_0}) \in [0, \frac{\pi}{2}]$, denoted by the subscript 0. These can be expressed for the incident beam as

$$\Psi_{in}(x,y) = \int_{-\infty}^{+\infty} dk_y\ f(k_y-k_{y_0})\ e^{i(k_{x1}(k_y)x+k_yy)}\begin{pmatrix}1\\ e^{i\phi_1(k_y)}\end{pmatrix} \tag{49}$$

as well as the reflected beam

$$\Psi_{re}(x,y) = \int_{-\infty}^{+\infty} dk_y\ r_s(k_y)\ f(k_y-k_{y_0})\ e^{i(-k_{x1}(k_y)x+k_yy)}\begin{pmatrix}1\\ -e^{-i\phi_1(k_y)}\end{pmatrix} \tag{50}$$

and the reflection amplitude is

$$r_s(k_y) = |r_s| e^{i\varphi_{r_s}} \tag{51}$$

this fact is represented by writing the x-component of wave vector k_{x1} as well as ϕ_1 both as function of k_y, where each spinor plane wave is a solution of (4). The function $f(k_y - k_{y_0})$ is the angular spectral distribution, which can be assumed of Gaussian shape

$$f(k_y - k_{y_0}) = w_y e^{-w_y^2 (k_y - k_{y_0})^2} \tag{52}$$

with w_y is the half beam width at waist [10]. We can approximate the k_y-dependent terms by a Taylor expansion around k_y and retaining only the first order term to get for the phase

$$\phi_1(k_y) \approx \phi_1(k_{y_0}) + \frac{\partial \phi_1}{\partial k_y}\Big|_{k_{y_0}} (k_y - k_{y_0}) \tag{53}$$

and also for the wave vector

$$k_{x1}(k_y) \approx k_{x1}(k_{y_0}) + \frac{\partial k_{x1}}{\partial k_y}\Big|_{k_{y_0}} (k_y - k_{y_0}). \tag{54}$$

As far as the transmission waves is concerned, we write the beam as

$$\Psi_{tr}(x,y) \;\; = \;\; \int_{-\infty}^{+\infty} dk_y \; t_s(k_y) \; f(k_y - k_{y_0}) \; e^{i(k_{x1}(k_y)x + k_y y)} \begin{pmatrix} 1 \\ e^{i\phi_1(k_y)} \end{pmatrix} \tag{55}$$

and the transmission amplitude is

$$t_s(k_y) = |t_s| e^{i\varphi_{t_s}} \tag{56}$$

which will be calculated through the use of the boundary conditions. The stationary-phase approximation indicates that the GHL shifts are equal to the negative gradient of transmission phase with respect to k_y. To calculate the GHL shifts of the transmitted beam through our system, according to the stationary phase method [13], we adopt the definition [5, 14, 15]

$$S_t = -\frac{\partial \varphi_{t_s}}{\partial k_y}\Big|_{k_{y0}}, \qquad S_r = -\frac{\partial \varphi_{r_s}}{\partial k_y}\Big|_{k_{y0}}. \tag{57}$$

These can be used to write the reflection and transmission probabilities as

$$T_s = |t_s|^2, \qquad R_s = |r_s|^2. \tag{58}$$

Obviously, we can check that the probability conservation condition $T_s + R_s = 1$ is well satisfied. Having obtained the closed form expressions of the GHL shifts and transmission in different energy domains, we proceed now to compute these quantities numerically. This will help us understand the effect of various potential parameters on the GHL shifts in our double linear barrier potential.

4 Discussion of numerical results

The physics of particle scattering through a linear double barrier depends on the energy of the incoming particle. We numerically evaluate the GHL shifts in transmission S_t and in reflection S_r as a function of structural parameters of the graphene double linear barrier, including the energy ϵ, the y-component

of the wave vector k_y, the energy gap μ and the potentials v_1 and v_2. To understand their behaviors, let us consider Figure 2(a) where we study the GHL shifts in transmission as well as the GHL shifts in reflection versus the energy ϵ for specific values of the parameters $d_1 = 1$, $d_2 = 2.5$, $v_1 = 60$, $v_2 = 30$. It was found that the GHL shifts can be negative as well as positive and become zero at transmission resonances in Figure 2(b). However, in intervals $\epsilon \leq v_2 - k_y$ and $v_2 + k_y \leq \epsilon \leq v_1$, there are oscillation resonances due to the Klein regime, that is, a situation in which only oscillatory solutions exist throughout and where the so called Klein paradox reigns. Finally in the interval where $\epsilon > v_1$ the usual high energy barrier oscillations and asymptotically the transmission reaches unity at high energy.

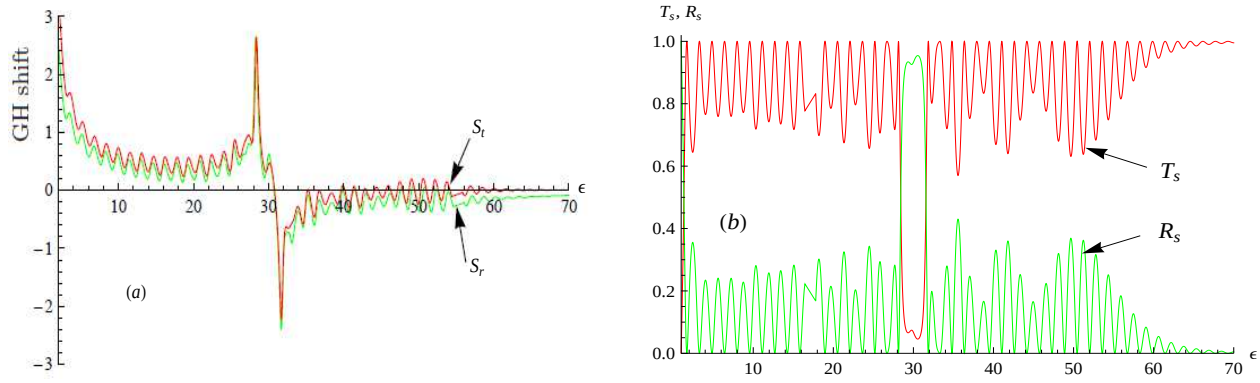

Figure 2: (Color online) (a): GHL shifts in transmission S_t and in reflection S_r as a function of energy ϵ. (b): Transmission and reflection probabilities (T_s, R_s) as a function of energy ϵ with $d_1 = 1$, $d_2 = 2.5$, $\mu = 0$, $k_y = 1$, $v_1 = 60$ and $v_2 = 30$.

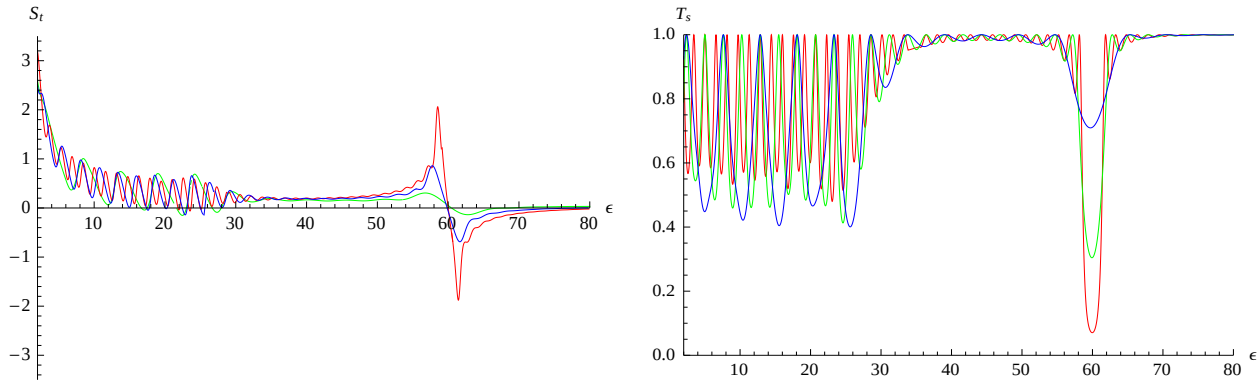

Figure 3: (Color online) (a): GHL shifts S_t in transmission. (b): The transmission probability T_s as a function of energy ϵ with $d_1 = 0.3$ (blue color), $d_1 = 0.6$ (green color), $d_1 = 1$ (red color), $d_2 = 2.5$, $\mu = 0$ and $k_y = 1$, $v_1 = 30$, $v_2 = 60$.

In Figure 3 we plot the GHL shifts 3(a) and transmission 3(b) as a function of the energy for specific values of the potential parameters $d_1 = 1$, $d_2 = 2.5$, $k_y = 1$, $v_1 = 30$ and $v_2 = 60$. It is clear from Figure 3(a) that the GHL shifts change sign at the Dirac points ($\epsilon = v_1$, $\epsilon = v_2$). We deduce that there is a strong dependence of the GHL shifts on d_1, it increases with d_1. However, in the energy domain $\epsilon < v_1$ the GHL shifts are positive as long as the energy satisfies the condition $v_1 < \epsilon < v_2$

and negative for $\epsilon > v_2$. We notice that the GHL shifts display sharp peaks inside the transmission gap around the point $\epsilon = v_1$, while they are absent around the energy point $\epsilon = v_2$. In such situation, one can clearly end up with an interesting result such that the number of sharp peaks is equal of that of transmission resonances. We also observe that the shifts become constant beyond certain energy threshold, which is compatible with a maximum of transmission.

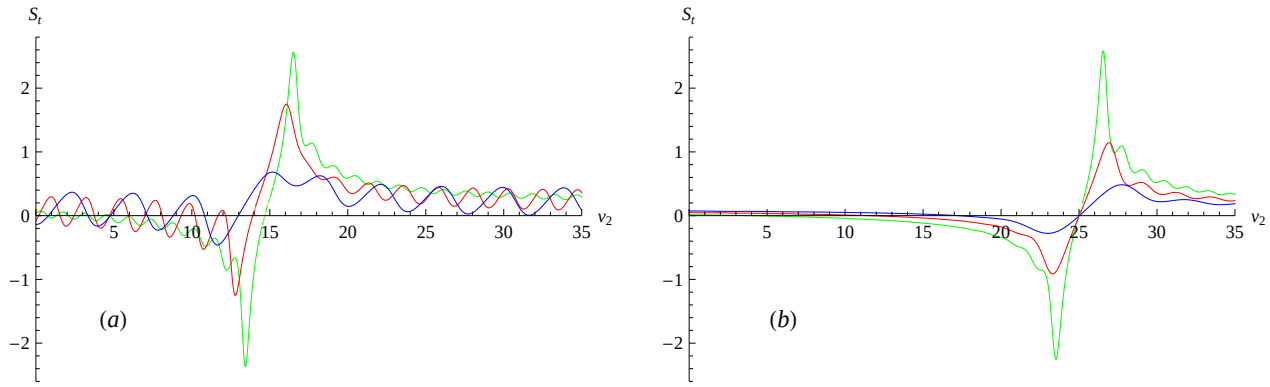

Figure 4: (Color online) GHL shift S_t as a function of energy potential v_2 with $d_1 = 0.4$ (blue color), $d_1 = 0.7$ (red color), $d_1 = 1.1$ (green color), $d_2 = 1.3$, $\mu = 0$, $k_y = 1$, $\epsilon = 15$ and $v_1 = 30$.

We show in Figure 4 the transmission versus potential strength v_2. We have chosen the parameters ($\epsilon = 15$, $v_1 = 25$) in Figure 4(a) and ($\epsilon = 25$, $v_1 = 15$) in Figure 4(b), with inter-barrier distance $d_2 = 1.3$ and distances $d_1 = \{0.4, 0.7, 1.1\}$. One can notice that, at the Dirac points $v_2 = \epsilon$, the GHL shifts change their sign. This change in sign of the GHL shifts shows clearly that they are strongly dependent on the barrier heights. We also notice that the GHL shifts are negative and positive in Figures 4(a) and 4(b). Note that, the Dirac points represent the zero modes for Dirac operator [8] and lead to the emergence of new Dirac points, which have been discussed in different works [21,22]. Such point separates the two regions of positive and negative refraction. In the cases of $v_2 < \epsilon$ and $v_2 > \epsilon$ (respectively $v_1 < \epsilon$ and $v_1 > \epsilon$), the shifts are respectively in the forward and backward directions, due to the fact that the signs of group velocity are opposite.

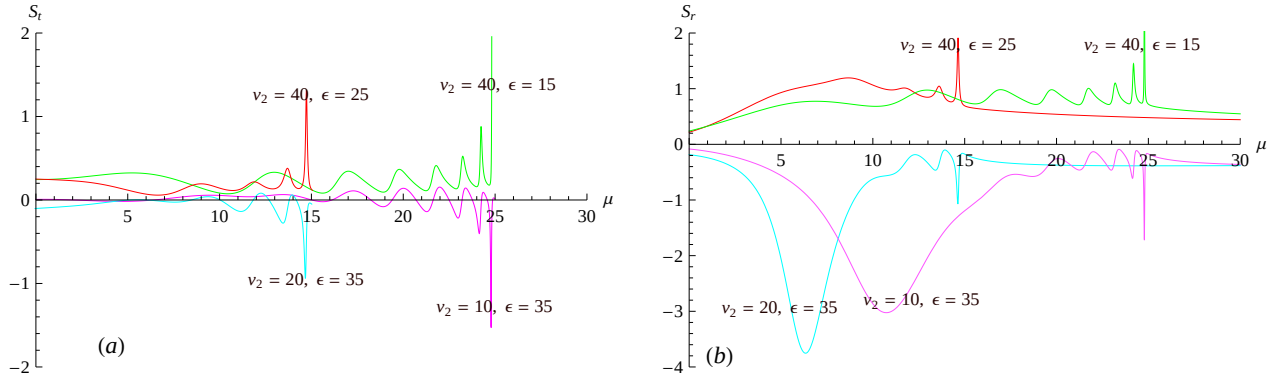

Figure 5: (Color online) (a)/(b): the GH in transmission and in reflection (S_r/S_r) as a function of energy gap μ with $d_1 = 0.5$, $k_y = 1$, $d_2 = 1.5$ and $v_1 = 50$, $\{v_2 = 40, \epsilon = 15\}$, $\{v_2 = 40, \epsilon = 25\}$, $\{v_2 = 10, \epsilon = 35\}$ and $\{v_2 = 20, \epsilon = 35\}$.

Now let us investigate what will happen if we introduce a gap in the intermediate region $x \leq |d_1|$. Note that, the gap is introduced as shown in Figure 1 and therefore it affects the system energy according to the solution of the energy spectrum obtained in region 3. Figure 5(a) and 5(b) show that the GHL shifts in the propagating case can be enhanced by a gap opening at the Dirac point. This has been performed by fixing the parameters $d_1 = 0.5$, $d_2 = 1.5$, $k_y = 1$, $v_1 = 50$ and making different choices for the energy ϵ and potential v_2. For $s_3 = \text{sign}(\epsilon - v_2) = 1$ we conclude that one can still have negative shifts. Note that (17) implies that for certain energy gap μ, there is no possible transmission. In fact, under the condition $\mu > |\epsilon - v_2|$ every incoming state is reflected. We notice that the GHL shifts in transmission S_t vanish for values of ϵ below the critical value $\mu = |\epsilon - v_2|$. Figure 5(b) shows the GHL shifts in reflection S_r as a function of energy gap μ. For the configuration $\{v_2 = 40; \epsilon = 15, 25\}$, we can still have positive shifts while for configuration $\{\epsilon = 35; v_2 = 10, 20\}$ the GHL shifts are negative. We notice that the GHL shifts in reflection S_r did not vanish and decreases with increasing μ for $s_3 = \text{sign}(\epsilon - v_2) = -1$ as well as increases with increasing μ for $s_3 = \text{sign}(\epsilon - v_2) = 1$.

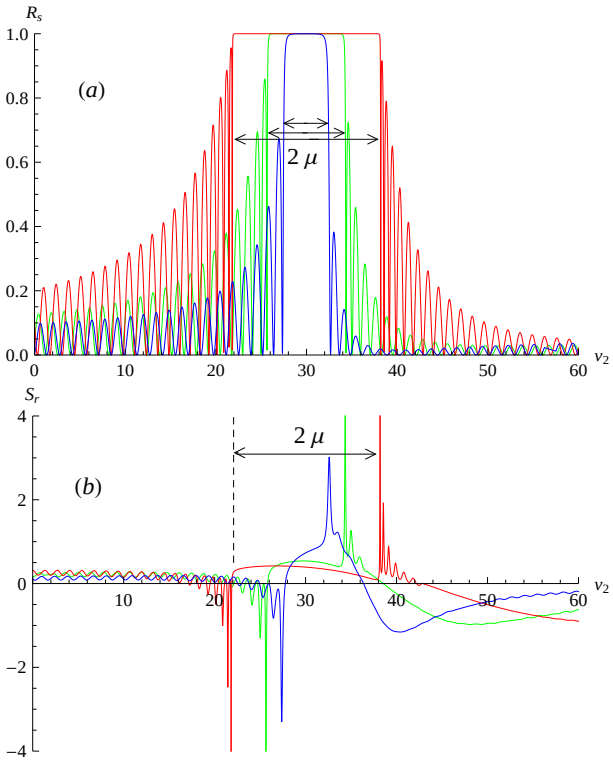

Figure 6: (Color online) (a): The reflection probability R_s and (b): the GHL shifts in reflection S_r as a function of energy gap μ with $d_1 = 1.1$, $k_y = 1$, $d_2 = 1.3$ and $v_1 = 50$, $\epsilon = 35$ and $\mu = 2, 4, 8$.

The above GHL shifts S_r and reflection probability R_s as function of potential strength v_2 for different values of the energy gaps μ are shown in Figure 6(a) and 6(b). From these Figures, we can see that the region of the weak GHL shifts become wide with the increase in energy gap μ, the shifts are affected by the internal structure of the double barrier. In particular it change the sign at the total reflection energies and peaks at each bound state associated with the double linear barrier. Thus the GHL shifts can be enhanced by the presence of resonant energies in the system when the

incident angle is less than the critical angle associated with total reflection. It is clearly seen that S_t is oscillating between negative and positive values around the critical point $v_2 = \epsilon$. At such point R_s is showing total reflection while it oscillates away from the critical point.

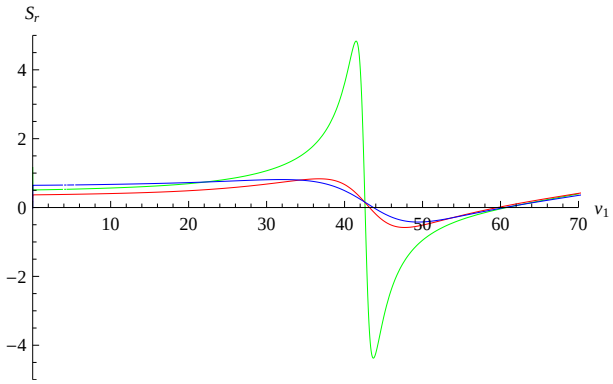

Figure 7: (Color online) the GHL shifts in reflection (S_r) as a function of energy gap μ with $d_1 = 1.1$, $k_y = 1$, $d_2 = 1.3$ and $v_1 = 50$, $\epsilon = 30$ and $\mu = 2, 4, 8$.

We show in Figure 7 the GHL shifts for the reflection versus potential strength v_1 for different energy gaps μ. One observes that the GHL shifts in reflection can be negative or positive. Therefore, we can control the positive and negative GHL shifts by changing the y-directional of the energy gap μ. In other words, we can control the moving directions of the carriers at the interface of the graphene barrier by adjusting μ.

5 Conclusion

In this paper we have considered a model to describe over-barrier electron emission from the edge of monolayer graphene through a linear electrostatic double barriers. We have computed the Goos-Hänchen like (GHL) shifts through a double barrier potential, the massless Dirac-like equation was used to describe the scattered fermions by such a potential configuration.

Our results showed that the GHL shifts are affected by the internal structure of the double barrier. In particular the GHL shifts change sign at the transmission zeroes and peaks at each bound state associated with the double barrier. Thus our numerical results showed that the GHL shifts can be enhanced in the presence of resonant energies in the system when the incident angle is less than the critical angle associated with total reflection.

Finally we close our work by mentioning some challenges facing the potential connection between the two fields, quantum optics and graphene. Very recently, pertinent discussions have been made to emphasis the main difficulties in detecting the GHL shifts and preparing the electron beam in solid-state physics [23]. These discussions open for us important research avenues that will help us understand and overcome the above mentioned difficulties. On the other hand, we learned from [23] that the spin-orbit coupling in optics is an interesting and fascinating topic because the spin-orbit interaction in graphene opens up a spin-orbit gap, though very small, at the Dirac points. All these matters will be highly important when we consider tunable GH shift leading to potential applications in future graphene based electronic devices. These matters will be investigated in the near future to

enable us to get a deeper understanding of graphene transport properties.

Acknowledgments

The generous support provided by the Saudi Center for Theoretical Physics (SCTP) is highly appreciated by all authors. AH and HB acknowledge the support of King Fahd University of Petroleum and minerals under research group project entitled "Transport Properties of Systems Composed of Coupled and Decoupled Graphene Flakes".

References

[1] K. S. Novoselov, A. K. Geim, S. V. Morozov, D. Jiang, Y. Zhang, S. V. Dubonos, I. V. Grigorieva and A. A. Firsov, Science 306, 666 (2004).

[2] F. Goos and H. Hänchen, Ann. Phys. 436, 333 (1947).

[3] F. Goos and H. Hänchen, Ann. Phys. 6, 251 (1949).

[4] K. Artmann, Ann. Phusik 2, 87 (1949).

[5] X. Chen, J.-W. Tao and Y. Ban, Eur. Phys. J. B 79, 203 (2011).

[6] Y. Song, H-C. Wu and Y. Guo, Appl. Phys. Lett. 100, 253116 (2012).

[7] X. Chen, P-L. Zhao, X-J. Lu and L-G. Wang, Eur. Phys. J. B 86, 223 (2013).

[8] M. Sharma and S. J. Ghosh, J. Phys.: Condens. Matter 23, 055501 (2011).

[9] J.-H. Huang, Z.-L. Duan, H.-Y. Ling and W.-P. Zhang, Phys. Rev. A 77, 063608 (2008).

[10] C. W. J. Beenakker, R. A. Sepkhanov, A. R. Akhmerov and J. Tworzydlo, Phys. Rev. Lett. 102, 146804 (2009).

[11] L. Zhao and S. F. Yelin, Phys. Rev. B 81, 115441 (2010).

[12] M. Mekkaoui, A. Jellal and H. Bahlouli, arXiv:1511.06880 (2015).

[13] D. Bohm, Quantum Theory, Prentice-Hall (New York, 1951), pp. 257-261.

[14] A. Jellal, I. Redouani, Y. Zahidi and H. Bahlouli, Phys. E 58, 30 (2014).

[15] A. Jellal, Y. Wang, Y. Zahidi and M. Mekkaoui, Phys. E 68, 53 (2015).

[16] A. Matulis, F. M. Peeters and P. Vasilopoulos, Phys. Rev. Lett. 72, 1518 (1994).

[17] M. Ramezani Masir, P. Vasilopoulos and F.M. Peeters, Phys. Rev. B 82, 115417 (2010).

[18] J. Tworzydlo, B. Trauzettel, M. Titov, A. Rycerz and C. W. J. Beenakker, Phys. Rev. Lett. 96, 246802 (2006).

[19] M. Abramowitz and I. Stegum, Handbook of Integrabls, Se ries and Products, (Dover, New York, 1956).

[20] L. Gonzalez-Diaz and V. M. Villalba, Phys. Lett. A 352, 202 (2006).

[21] S. Bhattacharjee, M. Maiti and K. Sengupta, Phys. Rev. B 76, 184514 (2007).

[22] C. H. Park, L. Yang, Y. W. Son, M. L. Cohen and S. G.Louie, Phys. Rev. Lett. 101, 126804 (2008).

[23] X. Chen, X.-J. Lu, Y. Ban and C.-F. Li, J. Opt. 15, 033001 (2013).

[24] H. Bahlouli, E.B. Choubabi, A. EL Mouhafid and A. Jellal, Solid State Communications 151 (2011) 1309.

[25] M. V. Berry and R. J. Modragon, Proc. R. Soc. London Ser. A 412, 53 (1987).